ARTICLES
https://doi.org/10.1038/s41567-018-0400-9
nature physics

Synthesis of antisymmetric spin exchange interaction and chiral spin clusters in superconducting circuits

Da-Wei Wang[1,2,3*], Chao Song[1], Wei Feng[1,4], Han Cai[1], Da Xu[1], Hui Deng[5], Hekang Li[5,6], Dongning Zheng[3,5,6], Xiaobo Zhu[7*], H. Wang[1*], Shi-Yao Zhu[1,7] and Marlan O. Scully[2]

According to quantum mechanics, chiral states cannot be non-degenerate eingenstates of a parity-conserving Hamiltonian. This is in contradiction to the existence of chiral molecules—a fact known as as the Hund paradox[1]. The origin of molecular and biological chirality is conjectured to be related to parity-breaking interactions[2,3] or environmental decoherence[4], but a quantum superposition of two chiral molecular states with distinctive optical activities has never been observed[5]. To make progress in addressing these questions, it would be helpful to construct an artificial quantum system that breaks the parity symmetry and that can be prepared in a superposition of two chiral states. Here we report the synthesis of the parity-breaking antisymmetric spin exchange interaction in all-to-all connected superconducting circuits, which allows us to show various chiral spin dynamics in up to five-spin clusters. We also demonstrate the entanglement of up to five qubits in Greenberger–Horne–Zeilinger states based on a three-spin chiral logic gate. Our results are a step towards quantum simulation of magnetism with antisymmetric spin exhange interaction and quantum computation with chiral spin states.

Two conditions are needed for the experimental observation of a quantum superposition of different chiral states. First, the chiral states must have observables that characterize their chirality. Second, there must be controllable interactions between the two chiral states to prepare a quantum superposition. A suitable platform that satisfies these conditions is the superconducting circuit, which has been widely used in quantum simulation and quantum computation, and has advantageous tunability, flexibility and scalability[6,7]. In particular, chiral ground-state currents of interacting photons hosted by a three-qubit unit cell have been observed with a synthesized magnetic field[8], and many-body localization has been seen in a chain of nine qubits[9]. Furthermore, the ground-state energy of a three-atom molecule, BeH_2, has been calculated using a six-qubit superconducting quantum processor[10].

Recently, some of us have proposed[11] that chiral photon dynamics gated by a spin can be used to generate mesoscopic superposition states. Similarly, we show here that chiral spin currents and parallel logic operations with superpositions of chiral spin states can be engineered in a cluster of superconducting qubits, that is, spin-1/2 particles, connected by a bus resonator. The key to this relies on the synthesis of the antisymmetric spin exchange interaction (ASI), which is also called the Dzyaloshinskii–Moriya interaction[12,13] in condensed matter physics and plays a critical role in establishing exotic spin orders[14–20]. In contrast to the more conventional symmetric Heisenberg interaction, synthesis of the ASI between qubits is experimentally more challenging. A photonic gauge field with photon–photon interactions has a similar effect, but it raises the hardware complexity because extra circuit elements, such as tunable couplers, are required[8].

Without increasing the circuit complexity, here we propose and demonstrate an alternative method to synthesize ASI[8] by periodically modulating the transition frequencies of the superconducting qubits coupled to the same bus resonator. Our achieved ASI Hamiltonian, featuring all-to-all connectivity, violates parity symmetry but conserves time-reversal symmetry. The parity symmetry-breaking ensures chiral spin currents, while the conservation of time-reversal symmetry guarantees opposite chiral dynamics of two spin configurations. This property is analogous to the quantum spin Hall effect[21], where electrons with opposite spins travel in opposite directions on the edges of a topological insulator. We have observed chiral spin dynamics in various spin-1/2 clusters containing up to five spins, as well as chiral dynamics involving composite spin-1 particles. By preparing a superposition of spin states with opposite chiral dynamics, we first entangle three qubits in a Greenberger–Horne–Zeilinger (GHZ) state and then demonstrate its scalability to five qubits.

To describe the underlying physics, we first introduce a central concept in describing chiral spin configurations, the spin chirality[22–25]:

$$C_z = \frac{1}{2\sqrt{3}}\boldsymbol{\sigma}_1 \cdot (\boldsymbol{\sigma}_2 \times \boldsymbol{\sigma}_3) \quad (1)$$

where $\boldsymbol{\sigma}_j = \sigma_j^x \hat{\mathbf{x}} + \sigma_j^y \hat{\mathbf{y}} + \sigma_j^z \hat{\mathbf{z}}$ $(j = 1, 2, 3)$ is the Pauli vector for the jth spin. Here we only introduce the z component of the chirality vector for simplicity of presentation (see Supplementary Information for the perspective of viewing the chiral spin dynamics as the

[1]Interdisciplinary Center for Quantum Information, Department of Physics and State Key Laboratory of Modern Optical Instrumentation, Zhejiang University, Hangzhou, Zhejiang, China. [2]Institute of Quantum Science and Engineering, Texas A&M University, College Station, TX, USA. [3]CAS Center of Excellence in Topological Quantum Computation, Beijing, China. [4]Beijing Computational Science Research Center, Beijing, China. [5]Institute of Physics, Chinese Academy of Sciences, Beijing, China. [6]School of Physical Sciences, University of Chinese Academy of Sciences, Beijing, China. [7]Synergetic Innovation Center of Quantum Information and Quantum Physics, University of Science and Technology of China, Hefei, Anhui, China. *e-mail: dwwang@zju.edu.cn; xbzhu16@ustc.edu.cn; hhwang@zju.edu.cn

precession of the chirality vector). Classically, this quantity is proportional to the solid angle subtended by the three spins. With C_z as a Hamiltonian, the three classical spins precess around their central axis. In quantum mechanics, the dynamics follows a similar behaviour as shown by the exponential operator C_z, which permutes the three spin states in a chiral way, that is,

$$e^{-iC_z\theta/2}\,|s_1s_2s_3\rangle = |s_3s_1s_2\rangle \tag{2}$$

where $s_j=\uparrow$ or $\downarrow$ and $\theta=4\pi/3$. This operation is non-trivial only when one of the spin states is different from the other two (for example, $|\uparrow\downarrow\downarrow\rangle$ and $|\downarrow\uparrow\uparrow\rangle$).

The chirality operator C_z breaks both parity and time-reversal symmetry. To observe opposite chiral dynamics of the two configurations $|\uparrow\downarrow\downarrow\rangle$ and $|\downarrow\uparrow\uparrow\rangle$, we need a Hamiltonian that breaks parity symmetry but conserves time-reversal symmetry. The product of C_z and $S_z=\sum_{j=1}^{3}\sigma_j^z/2$ satisfies this requirement,

$$H=\hbar\kappa S_zC_z=\sum_{j=1}^{3}\mathbf{D}\cdot(\boldsymbol{\sigma}_j\times\boldsymbol{\sigma}_{j+1}) \tag{3}$$

where $\mathbf{D}=\hbar\kappa\hat{\mathbf{z}}/4\sqrt{3}$, with κ being a coupling constant and j running cyclically from 1 to 3. Equation (3) is a chiral ASI Hamiltonian of three spins (see Methods). The key feature of H is that the two subspaces with $S_z=\pm1/2$ have opposite chiral dynamics, that is,

$$\begin{aligned} e^{-iHT_0/\hbar}\,|\uparrow\downarrow\downarrow\rangle &= |\downarrow\downarrow\uparrow\rangle \\ e^{-iHT_0/\hbar}\,|\downarrow\uparrow\uparrow\rangle &= |\uparrow\downarrow\uparrow\rangle \end{aligned} \tag{4}$$

where $T_0\equiv\theta/\kappa=4\pi/3\kappa$. To understand this, we note that the two opposite chiral evolutions are time-reversal to each other.

The experimental results confirming the chiral dynamics in equation (4) are shown in Fig. 1. The experiment was performed on superconducting circuits containing five transmon qubits (Q_a to Q_e in Fig. 1a), interconnected by a central bus resonator (see Methods and Supplementary Information for more information on the device and experimental details). The three qubits $Q_dQ_bQ_a$ are in order assigned to the three spin sites $s_1s_2s_3$, as shown schematically in Fig. 1b. This chiral dynamics is reminiscent of the quantum spin Hall effect[21]. The three spins form a minuscule two-dimensional lattice with only edges, and the three eigenstates in each subspace $S_z=\pm1/2$ are chiral edge states of spin waves that host edge currents in opposite directions. To synthesize the ASI, we periodically modulate their transition frequencies around the resonance frequency of the bus resonator ω_r, while the other two of the five qubits are far detuned. The time-dependent transition frequencies of the three qubits are $\omega_j(t)=\omega_r+\Delta\cos(\nu t-\phi_j+\phi_0)$ with $\Delta/2\pi=235$ MHz, $\nu/2\pi=98.8$ MHz and $\phi_j=2j\pi/3$, and ϕ_0 is an initial phase. This modulation results in an effective Floquet Hamiltonian H in equation (3) with $\kappa=2\pi\times4.44$ MHz and $T_0=150$ ns. Here, subscript j refers to the spin site index.

The chiral dynamics of spin clusters containing four and five spins with the engineered ASI are shown in Figs. 2 and 3. Substantially unlike the symmetric interaction, ASI lifts the degeneracy of the eigenstates that are parity-symmetric to each other and allows a chiral evolution of the spin excitation over all spin sites in a sequence determined by the order of i and j in $\boldsymbol{\sigma}_j\times\boldsymbol{\sigma}_i$. In each of the triangular loops of Figs. 2a,d and 3a, the dynamics is similar to those shown in Fig. 1c,d.

Interestingly, for chiral dynamics involving four and five spins, we can take a different perspective by grouping two spin-1/2 sites as a composite spin-1 particle. In Fig. 2a,d, the four qubits $Q_aQ_bQ_cQ_e$ are in order assigned to the four spin sites $s_1s_2s_3s_4$, and the interaction

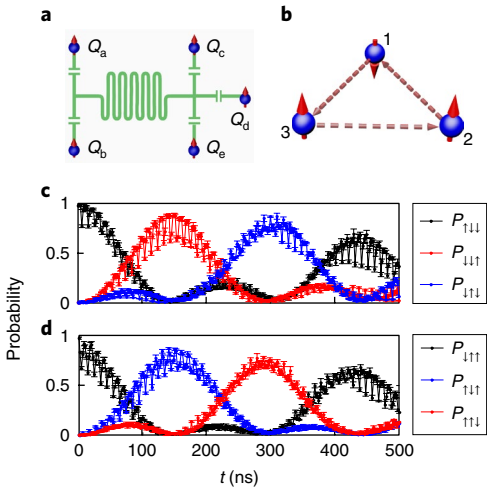

Fig. 1 | Three-spin chiral dynamics induced by synthesized ASI. a, Circuit schematic of five qubits connected to a bus resonator (central sinusoid line). **b**, Schematic of ASI between the three spins in equation (3). Dashed arrows from site i to site j (i, $j=1,2,3$) denote the interaction $\mathbf{D}\cdot(\boldsymbol{\sigma}_j\times\boldsymbol{\sigma}_i)$. **c**, Chiral dynamics with three spins $s_1s_2s_3$ initialized in $|\uparrow\downarrow\downarrow\rangle$. The time-dependent probabilities of the spin configurations are labelled. The spin-up state moves chirally from $1\rightarrow3\rightarrow2$. **d**, Chiral dynamics with the three spins initialized in $|\downarrow\uparrow\uparrow\rangle$. The spin-down state moves from $1\rightarrow2\rightarrow3$, with chirality opposite that of the case in **c**. The data are averaged over five datasets, and error bars represent the s.d. of these repeated sets of measurements. Neighbouring data points are connected by straight lines to show the fast oscillations due to modulation of the transition frequencies of the qubits. Numerical simulations are provided in the Supplementary Information.

Hamiltonian can be written as $H_1=\mathbf{D}\cdot(\mathbf{S}_1\times\boldsymbol{\sigma}_1+\boldsymbol{\sigma}_1\times\boldsymbol{\sigma}_4+\boldsymbol{\sigma}_4\times\mathbf{S}_1)$, with $\mathbf{S}_1=\boldsymbol{\sigma}_2+\boldsymbol{\sigma}_3$ being a composite spin-1 operator. This can be achieved by setting the modulation phases $\phi_1=0$, $\phi_2=\phi_3=-2\pi/3$ and $\phi_4=2\pi/3$. If we initialize $|s_1s_2s_3s_4\rangle$ in state $|\uparrow\downarrow\downarrow\downarrow\rangle$, the spin-up excitation chirally evolves to a superposition of the qubits on sites 2 and 3, then to site 4, and finally back to site 1, as shown in Fig. 2a–c. If we reverse the initial state of all spins, the chiral evolution has an opposite direction due to the time-reversal symmetry, as shown in Fig. 2d–f. The spin-1 operator $\mathbf{S}_1$ in H_1 provides extra freedom to control the chiral evolution. In the Supplementary Information, we show that we can freeze and recover the chiral spin dynamics and generate fully entangled states by quantum control of the intermediate states during the chiral evolution.

In Fig. 3a–c we show the chiral dynamics of a five-spin cluster where a central site interacts with four corner sites with synthesis of the nearest-neighbour ASI, obtained on another superconducting circuit with the same design and similar performance (see Supplementary Information). The five qubits $Q_cQ_aQ_dQ_bQ_e$ are in order assigned to the five spin sites $s_1s_2s_3s_4s_5$. The resulting Hamiltonian is $H_2=\mathbf{D}\cdot(\mathbf{S}_1\times\boldsymbol{\sigma}_1+\boldsymbol{\sigma}_1\times\mathbf{S}_2+\mathbf{S}_2\times\mathbf{S}_1)$ with $\mathbf{S}_2=\boldsymbol{\sigma}_4+\boldsymbol{\sigma}_5$, which can be regarded as a spin-1/2 interacting with two spin-1 particles. This Hamiltonian is achieved by setting $\phi_1=0$, $\phi_2=\phi_3=-2\pi/3$ and $\phi_4=\phi_5=2\pi/3$. In each of the triangles there still is a chiral evolution determined by the interaction order in ASI, such that the spin-up excitation first evolves from site 1 to a superposition of sites 2 and 3, then to a superposition of sites 4 and 5, and finally back to site 1.

We further note that, with the all-to-all device connectivity and the individual qubit tunability, we can achieve various configurations of ASI for different chiral spin dynamics by changing the modulation phases and amplitudes on each spin site. In Fig. 3d, we can choose the modulation phases $\phi_j=-2j\pi/5$ with

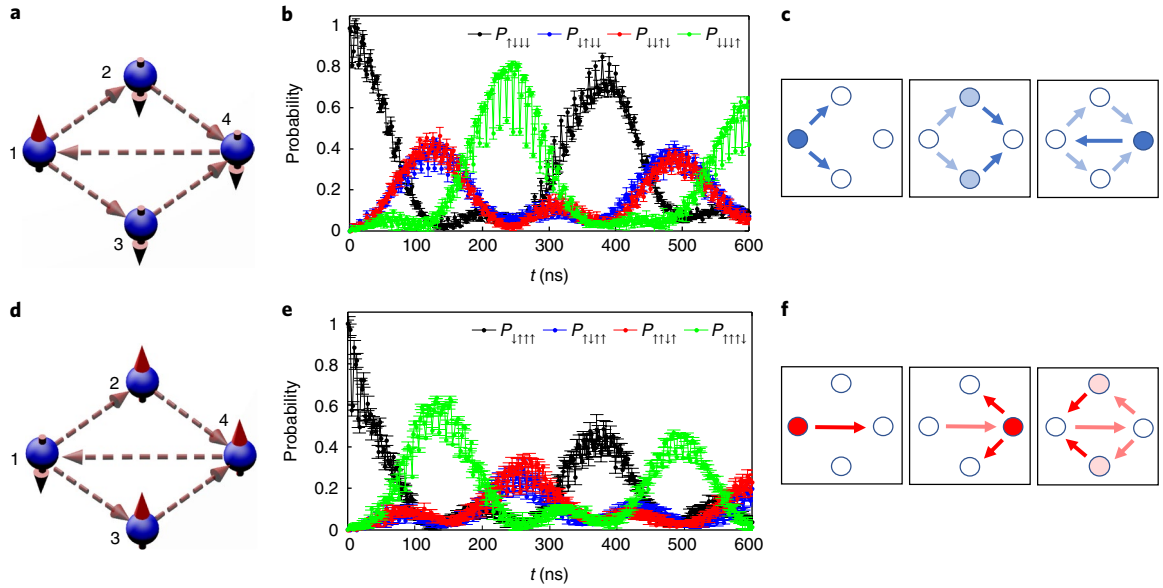

Fig. 2 | Chiral spin dynamics in a four-spin cluster. a, The initial spin configuration and the ASI between them. Dashed arrows between spins have the same meaning as in Fig. 1b. **b**, Evolution of the populations of the single spin-up states when the spins are initialized in state $|s_1s_2s_3s_4\rangle = |\uparrow\downarrow\downarrow\downarrow\rangle$. **c**, Illustration of the chiral evolution of a single spin-up excitation. **d**–**f**, Evolution of a single spin-down state with opposite chiral dynamics compared with a single spin-up state. Error bars represent s.d. of repeated sets of measurements. In **c** and **f**, the depth of the blue (red) colour in the circles represents the probabilities of the spin-up (spin-down) states. Dark blue (red) arrows show the evolution direction of the spin-up (spin-down) state. Light blue (red) arrows show the paths that the spin-up (spin-down) state has covered.

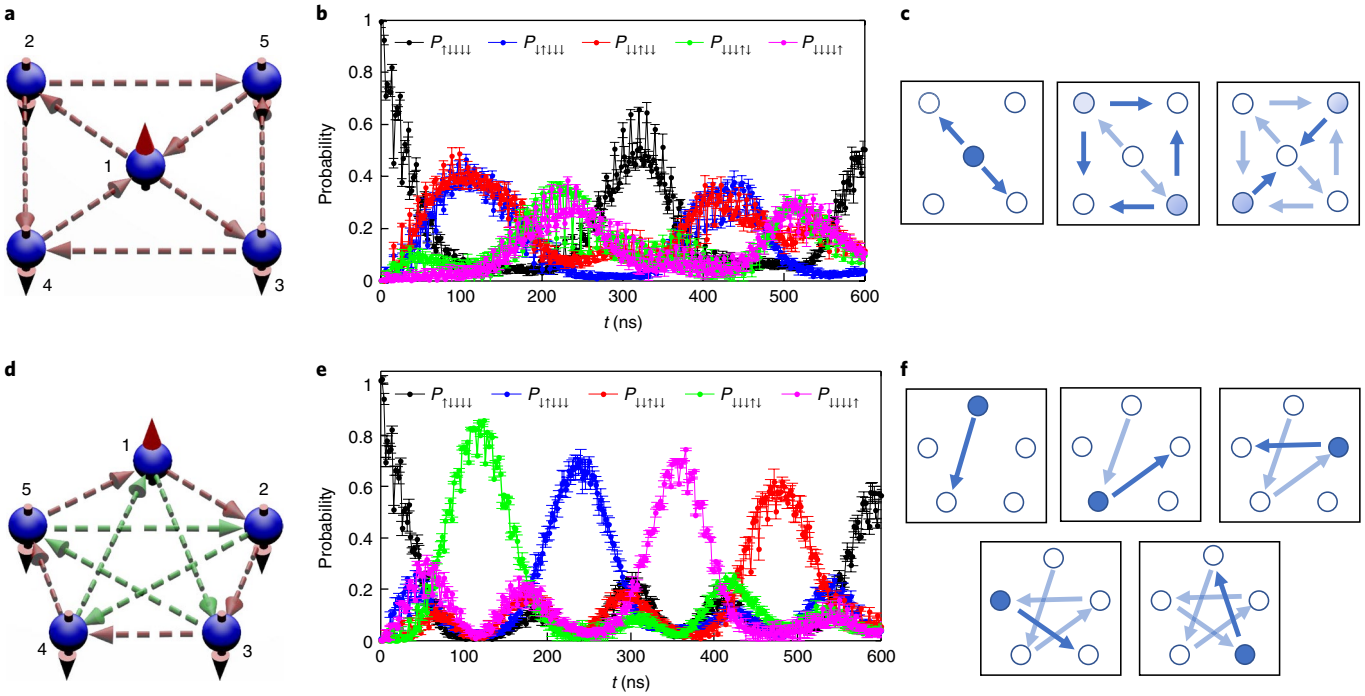

Fig. 3 | Chiral spin dynamics in a five-spin cluster. a, The five spins form four triangles sharing a central spin, which can be considered as the ASI among one spin-1/2 and two spin-1 particles. **b**, Probabilities of the five-spin states with one spin-up excitation are shown as functions of time. The spin-up state is transferred from 1 to a superposition state of 2 and 3, and then to a superposition state of 4 and 5, and finally back to 1, as schematically shown in **c**. **d**, The five spins form a pentagon featuring nearest-neighbour and next-nearest-neighbour ASI. **e**, Probabilities of the five-spin states in the chiral evolution. **f**, Schematic showing that the single spin-up state hops to the next-nearest neighbours chirally along the path $1\rightarrow4\rightarrow2\rightarrow5\rightarrow3\rightarrow1$. Error bars represent s.d. of the repeated sets of measurement. In **c** and **f** the meanings of the circles and arrows are as in Fig. 2c.

$j=1,2,\ldots,5$, for which $Q_cQ_eQ_bQ_dQ_a$ are in order assigned to the five spin sites $s_1s_2s_3s_4s_5$. The ASI Hamiltonian includes nearest-neighbour terms and those beyond the nearest neighbour, $H_3=\sum_j 1.97\mathbf{D}\cdot(\boldsymbol{\sigma}_j\times\boldsymbol{\sigma}_{j-1})+0.53\mathbf{D}\cdot(\boldsymbol{\sigma}_j\times\boldsymbol{\sigma}_{j-2})$, where j runs cyclically from 1 to 5 (see Methods). The ASI forms an all-to-all connected pentagon configuration that hosts a chiral evolution of a

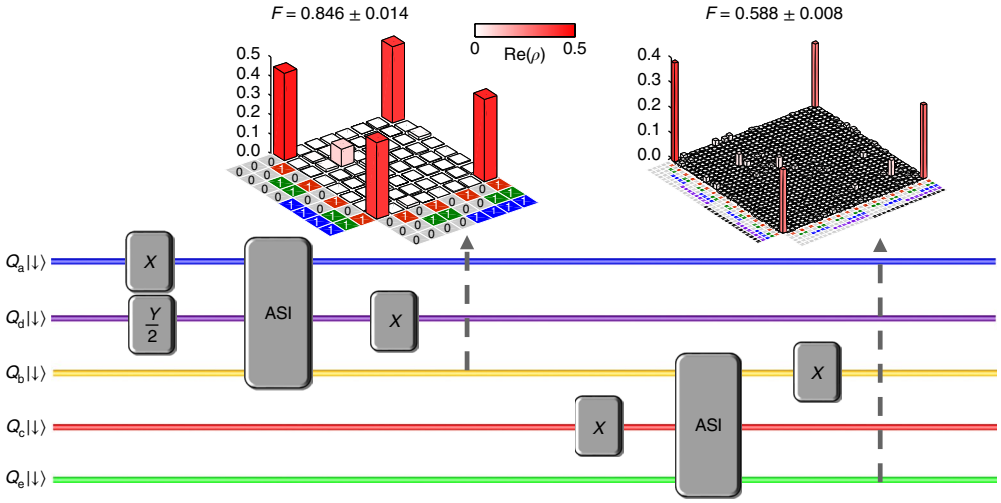

Fig. 4 | Generating GHZ states with ASI. In the quantum circuits, X is the π rotation gate around the $\hat{x}$ axis, $Y/2$ is the $\pi/2$ rotation gate around the $\hat{y}$ axis, and ASI is the three-spin chiral gate that transforms the states according to equation (4). F is the GHZ state fidelity. The colour bar is for Re(ρ), the real part of the density matrix, which has a negligible imaginary part (smaller than 0.021 and 0.045 for three- and five-qubit GHZ states, respectively).

single excitation along the sites $1\rightarrow4\rightarrow2\rightarrow5\rightarrow3\rightarrow1$, as shown in Fig. 3e and pictorially plotted in Fig. 3f. This evolution can be used in state transfer in quantum spin networks[26,27]. The sequential spin transfer results from interference among multiple quantum pathways, because at intermediate times all sites might have considerable occupation probabilities. By including both symmetric and antisymmetric spin exchange interactions, the sequential spin transfer can be extended to arbitrary spin numbers, although the experimental implementation is more complicated than for the cases of three (Fig. 1) and five spins (Fig. 3; see also Supplementary Information).

Chiral rotation of photons can be used to generate entanglement[11]. Similarly, with chiral spin states we can entangle three qubits in a GHZ state at a time and scale it to five qubits, as shown in Fig. 4 (see Methods). The fidelities of the three-qubit GHZ states prepared with spins $s_1s_2s_3$ and $s_3s_4s_5$ are 0.846 ± 0.014 and 0.877 ± 0.012, respectively. The fidelity of the five-qubit GHZ state is 0.588 ± 0.008, which satisfies the criteria for genuine entanglement. These fidelity values agree with numerical simulations, taking into account the control and coherence parameters (see Supplementary Information for the error budget).

Our experiment demonstrates a three-qubit chiral gate based on the synthesized ASI in superconducting circuits. Complementing the symmetric interactions, the synthesis of ASI in a commonly used superconducting circuit paves the way for simulating chiral magnetism. Quantum logic operations based on chiral spin states are of substantial interest in quantum information processing, because they offer an extra dimension for control with chirality[28] and may improve the device coherence metric with decoherence-free subspaces[29]. In particular, chiral spin states with chirality $+1$ and -1 are subradiant states, which may exhibit better coherence than single spin states[30]. Therefore, our work also provides a platform for quantum computation with chiral spin states. We further note that, based on devices with six or more qubits, we can access the rich chiral dynamics in the subspaces with higher excitation numbers of the spin-1 and larger spin systems. The dynamics of a large quantum system with a parity symmetry-breaking Hamiltonian, mesoscopic superposition states prepared through coherent control of the Hamiltonian, and the decoherence of the superposition states can also help us to understand the existence of chirality in general (for example, chiral chemical and biological molecules).

Online content

Any methods, additional references, Nature Research reporting summaries, source data, statements of data availability and associated accession codes are available at https://doi.org/10.1038/s41567-018-0400-9.

Received: 22 January 2018; Accepted: 6 December 2018;
Published online: 21 January 2019

References

1. Hund, F. Zur Deutung der Molekelspektren III. *Z. Physik* **43**, 805–826 (1927).
2. Mason, S. F. Origins of biomolecular handedness. *Nature* **311**, 19–23 (1984).
3. Darquie, B. et al. Progress toward the first observation of parity violation in chiral molecules by high-resolution laser spectroscopy. *Chirality* **22**, 870–884 (2010).
4. Trost, J. & Hornberger, K. Hund's paradox and the collisional stabilization of chiral molecules. *Phys. Rev. Lett.* **103**, 023202 (2009).
5. Cina, J. A. & Harris, R. A. Superpositions of handed wave functions. *Science* **267**, 832–833 (1995).
6. Houck, A. A., Tureci, H. E. & Koch, J. On-chip quantum simulation with superconducting circuits. *Nat. Phys.* **8**, 292–299 (2012).
7. Xiang, Z.-L., Ashhab, S., You, J. Q. & Nori, F. Hybrid quantum circuits: superconducting circuits interacting with other quantum systems. *Rev. Mod. Phys.* **85**, 623–653 (2013).
8. Roushan, P. et al. Chiral ground-state currents of interacting photons in a synthetic magnetic field. *Nat. Phys.* **13**, 146–151 (2017).
9. Roushan, P. et al. Spectroscopic signatures of localization with interacting photons in superconducting qubits. *Science* **358**, 1175–1179 (2017).
10. Kandala, A. et al. Hardware-efficient variational quantum eigensolver for small molecules and quantum magnets. *Nature* **549**, 242–246 (2017).
11. Wang, D.-W., Cai, H., Liu, R.-B. & Scully, M. O. Mesoscopic superposition states generated by synthetic spin–orbit interaction in Fock-state lattices. *Phys. Rev. Lett.* **116**, 220502 (2016).
12. Dzialoshinskii, I. E. Thermodynamic theory of weak ferromagnetism in antiferromagnetic substances. *J. Exp. Theoret. Phys.* **32**, 1547–1562 (1957).
13. Moriya, T. New mechanism of anisotropic superexchange interaction. *Phys. Rev. Lett.* **4**, 228–230 (1960).
14. Ma, X. et al. Dzyaloshinskii–Moriya interaction across an antiferromagnet–ferromagnet interface. *Phys. Rev. Lett.* **119**, 027202 (2017).
15. Mühlbauer, S. et al. Skyrmion lattice in a chiral magnet. *Science* **323**, 915–919 (2009).
16. Dmitrienko, V. E. et al. Measuring the Dzyaloshinskii–Moriya interaction in a weak ferromagnet. *Nat. Phys.* **10**, 202–206 (2014).
17. Emori, S., Bauer, U., Ahn, S.-M., Martinez, E. & Beach, G. S. D. Current-driven dynamics of chiral ferromagnetic domain walls. *Nat. Mater.* **12**, 611–616 (2013).
18. Takagi, R. et al. Spin-wave spectroscopy of the Dzyaloshinskii–Moriya interaction in room-temperature chiral magnets hosting skyrmions. *Phys. Rev. B* **95**, 220406 (2017).

19. Heinze, S. et al. Spontaneous atomic-scale magnetic skyrmion lattice in two dimensions. *Nat. Phys.* **7**, 713–718 (2011).
20. Nagaosa, N. & Tokura, Y. Topological properties and dynamics of magnetic skyrmions. *Nat. Nanotechnol.* **8**, 899–911 (2013).
21. Kane, C. L. & Mele, E. J. Quantum spin Hall effect in graphene. *Phys. Rev. Lett.* **95**, 226801 (2005).
22. Wen, X. G., Wilczek, F. & Zee, A. Chiral spin states and superconductivity. *Phys. Rev. B* **39**, 11413–11423 (1989).
23. Grohol, D. et al. Spin chirality on a two-dimensional frustrated lattice. *Nat. Mater.* **4**, 323–328 (2005).
24. Taguchi, Y., Oohara, Y., Yoshizawa, H., Nagaosa, N. & Tokura, Y. Spin chirality, Berry phase, and anomalous Hall effect in a frustrated ferromagnet. *Science* **291**, 2573–2576 (2001).
25. Trif, M., Troiani, F., Stepanenko, D. & Loss, D. Spin–electric coupling in molecular magnets. *Phys. Rev. Lett.* **101**, 217201 (2008).
26. Christandl, M., Datta, N., Ekert, A. & Landahl, A. J. Perfect state transfer in quantum spin networks. *Phys. Rev. Lett.* **92**, 187902 (2004).
27. Eldredge, Z. et al. Fast quantum state transfer and entanglement renormalization using long-range interactions. *Phys. Rev. Lett.* **119**, 170503 (2017).
28. Georgeot, B. & Mila, F. Chirality of triangular antiferromagnetic clusters as a qubit. *Phys. Rev. Lett.* **104**, 200502 (2010).
29. Scarola, V. W., Park, K. & Sarma, S. D. Chirality in quantum computation with spin cluster qubits. *Phys. Rev. Lett.* **93**, 120503 (2004).
30. Scully, M. O. Single photon subradiance: quantum control of spontaneous emission and ultrafast readout. *Phys. Rev. Lett.* **115**, 243602 (2015).

Acknowledgements

The authors thank W. Liu, Q. Guo and K. Huang for technical support. This research was supported by the National Key Research and Development Program of China (grants nos. 2018YFA0307200, 2017YFA0304202 and 2016YFA0300601), the National Natural Science Foundations of China (grants nos. 11434008, 11574380, 11725419 and 11874322) and the Fundamental Research Funds for the Central Universities of China (grant no. 2016XZZX002-01). D.W.W. was also supported by the key research programme of the Chinese Academy of Sciences (grant no. XDPB08-3). M.O.S. was supported by the Air Force Office of Scientific Research (award no. FA9550-18-1-0141), the Office of Naval Research (award no. N00014-16-1-3054) and the Robert A. Welch Foundation (grant no. A-1261). Devices were made at the Nanofabrication Facilities at the Institute of Physics in Beijing, the University of Science and Technology of China in Hefei and the National Center for Nanoscience and Technology in Beijing.

Author contributions

D.W.W. conceived the idea and formulated the theory. D.W.W. and H.W. planned the project. C.S. performed the experiments. W.F., H.C. and C.S. carried out the simulation and analysed the data. H.D., H.L., D.Z. and X.Z. fabricated the sample with designs and support from H.W.'s group. D.X. provided technical support. D.W.W., W.F. and H.W. wrote the paper and S.Y.Z. and M.O.S. made comments.

Competing interests

The authors declare no competing interests.

Additional information

Supplementary information is available for this paper at https://doi.org/10.1038/s41567-018-0400-9.

Reprints and permissions information is available at www.nature.com/reprints.

Correspondence and requests for materials should be addressed to D.-W.W., X.Z. or H.W.

Publisher's note: Springer Nature remains neutral with regard to jurisdictional claims in published maps and institutional affiliations.

Methods

Device information. Our devices consist of multiple transmon qubits[31] that are symmetrically coupled to a central bus resonator[32]. The transition frequency of each qubit can be individually tuned through its Z bias line, while that of the bus resonator is fixed at ω_r around 5.6 GHz. The on-resonant coupling between each qubit and the resonator is ~20 MHz. Qubit energy relaxation times T_1 are in the range of 10–20 μs and dephasing times T_2^* relevant to the experimental data are in the range of 1–3 μs (see Supplementary Information).

The effective Hamiltonian. The interaction Hamiltonian of three qubits coupled with the same resonator under the rotating wave approximation is

$$H_1 = \hbar \sum_{j=1}^{3} (g_j a^\dagger \sigma_j^- e^{-if\sin(\nu t-\phi_j+\phi_0)} + \text{h.c.}) \quad (5)$$

where $a^\dagger$ and a are the creation and annihilation operators of the resonator mode, g_j is the coupling strength between the jth spin and the resonator, and $f=\Delta/\nu$. The central frequencies of the qubits are equal to ω_r. Under the condition $\nu \gg g_j$, we obtain the effective Floquet Hamiltonian[33,34], $H_I = H_0 + H$, where $H_0 = \hbar J_0(f) \sum_{j=1}^{3} (g_j a^\dagger \sigma_j^- + \text{h.c.})$, and the ASI Hamiltonian,

$$H = \frac{\hbar}{2\sqrt{3}} \sum_{j=1}^{3} (i\kappa_{j,(j+1)}\sigma_j^+\sigma_{j+1}^- - i\kappa_{j,(j+1)}^*\sigma_{j+1}^+\sigma_j^-) \quad (6)$$

with $\kappa_{j,(j+1)} = 2\sqrt{3} g_j^* g_{j+1} \beta / \nu$ and $\beta = \sum_{n=1}^{\infty} 2J_n^2(f)\sin[n(\phi_{j+1}-\phi_j)] / n$, where j and $j+1$ are cyclic from 1 to 3. Here $J_n(f)$ is the nth-order Bessel function of the first kind. Due to the imperfect fabrication, the qubit–resonator coupling strength g_j varies slightly from the designed value of 20 MHz (see Supplementary Information). For the sake of analytic simplicity, here we assume a homogeneous coupling strength, that is, $g_j \equiv 20$ MHz and $\kappa_{j,(j+1)} \equiv \kappa$. Ideally, when $f=2.40$, $J_0(f)=0$ and $\phi_j = 2j\pi/3$, we obtain $H_0 = 0$, $H_I = H$ in equation (3), with $\beta \approx 0.307$, $\kappa = 2\pi \times 4.29$ MHz and $T_0 = 155$ ns. However, due to the higher-order terms in the Hamiltonian, $H_I = H$ is realized in the two subspaces with slightly different parameters, $\nu/2\pi = 98.0$ MHz for $S_z = -1/2$ and 99.8 MHz for $S_z = 1/2$. In the experiment, we use $\nu/2\pi = 98.8$ MHz to reconcile simultaneous chiral rotations in the two subspaces with $\kappa = 2\pi \times 4.44$ MHz, $f=2.38$ and $T_0 = 150$ ns.

In Fig. 3d–f, the modulation phases of the five spins are $\phi_j = -2j\pi/5$ with $j = 1, 2, ..., 5$. The ASI between nearest neighbours has a factor $\beta_1 = \sum_{n=1}^{\infty} 2J_n^2(f)\sin(2n\pi/5)/n = 0.605 = 1.97\beta$, while the ASI between the next-nearest neighbours has a factor $\beta_2 = \sum_{n=1}^{\infty} 2J_n^2(f)\sin(4n\pi/5)/n = 0.163 = 0.53\beta$. This results in the numerical factors in the two terms of the Hamiltonian $H_3 = \sum_j 1.97\mathbf{D}\cdot(\boldsymbol{\sigma}_j \times \boldsymbol{\sigma}_{j-1}) + 0.53\mathbf{D}\cdot(\boldsymbol{\sigma}_j \times \boldsymbol{\sigma}_{j-2})$ in the main text.

Gauge invariance. The Hamiltonian in equation (6) indicates that a phase factor i or $-i$ is gained during each spin exchange transition. The chiral spin dynamics is determined by the total phase accumulated in transitions along a closed loop of the three qubits, which is $\pm\pi/2$ and gauge-invariant[8,35]. This gauge invariance is also valid for any closed loop in more complex spin-cluster patterns, as shown in Figs. 2 and 3 (see Supplementary Information).

Procedure for generating GHZ states. Starting with the state for the first three spin sites $s_1 s_2 s_3$ that host $Q_a Q_d Q_b$, we flip s_1 and apply a $\pi/2$ rotation to s_2, which results in the wavefunction $|\Psi(0)\rangle = (|\uparrow\downarrow\downarrow\rangle + |\uparrow\uparrow\downarrow\rangle)/\sqrt{2}$. We then turn on the ASI Hamiltonian for time T_0. Due to the opposite chiral dynamics of the two component states, the wavefunction evolves to $|\Psi(T_0)\rangle = (|\downarrow\uparrow\downarrow\rangle + |\uparrow\downarrow\uparrow\rangle)/\sqrt{2}$. This step is a three-spin chiral logic gate, as labelled 'ASI' in Fig. 4. We then apply a π rotation to s_2 and obtain a three-qubit GHZ state. The scalability of this scheme is demonstrated by including two additional spin sites $s_4 s_5$, which host $Q_c Q_e$, in the state $|\uparrow\downarrow\rangle$, and therefore the five-spin state is $|\Psi(T_0)\rangle = (|\downarrow\downarrow\downarrow\uparrow\downarrow\rangle + |\uparrow\uparrow\uparrow\uparrow\downarrow\rangle)/\sqrt{2}$. Now we apply the three-spin chiral logic gate on $s_3 s_4 s_5$, which results in the state $|\Psi(2T_0)\rangle = (|\downarrow\downarrow\uparrow\downarrow\downarrow\rangle + |\uparrow\uparrow\downarrow\uparrow\uparrow\rangle)/\sqrt{2}$. We then apply a π rotation to s_3 to prepare a five-qubit GHZ state. The fidelities of the three- and five-qubit GHZ states generated in the experiment exceed 0.5, indicating the existence of genuine entanglement[36].

Data availability

The data that support the plots within this paper and other findings of this study are available from the corresponding authors upon reasonable request.

References

31. DiCarlo, L. et al. Demonstration of two-qubit algorithms with a superconducting quantum processor. *Nature* **460**, 240–244 (2009).
32. Song, C. et al. 10-qubit entanglement and parallel logic operations with a superconducting circuit. *Phys. Rev. Lett.* **119**, 180511 (2017).
33. Kyriienko, O. & Sorensen, A. S. Floquet quantum simulation with superconducting qubits. *Phys. Rev. Appl.* **9**, 064029 (2018).
34. Wu, Y. et al. An efficient and compact switch for quantum circuits. *npj Quantum Inf.* **4**, 50 (2018).
35. Koch, J., Houck, A. A., Hur, K. L. & Girvin, S. M. Time-reversal-symmetry breaking in circuit-QED-based photon lattices. *Phys. Rev. A* **82**, 043811 (2010).
36. Otfried, G. & Seevinck, M. Separability criteria for genuine multiparticle entanglement. *New J. Phys.* **12**, 053002 (2010).